Inorganica Chimica Acta 413 (2014) 174–186

Contents lists available at ScienceDirect

Inorganica Chimica Acta

journal homepage: www.elsevier.com/locate/ica

Synthesis, crystal structures, DNA binding and cleavage activity of water soluble mono and dinuclear copper(II) complexes with tridentate ligands

Madur Pragathi [1], Katreddi Hussain Reddy *

Department of Chemistry, Sri Krishnadevaraya University, Anantapur 515003, Andhra Pradesh, India

ARTICLE INFO

Article history:
Received 20 May 2013
Received in revised form 16 January 2014
Accepted 16 January 2014
Available online 24 January 2014

Keywords:
Water soluble mono and dinuclear copper(II) complexes
Tridentate
Absorption spectrophotometry
Nuclease activity
Gel electrophoresis

ABSTRACT

Water soluble mono and dinuclear copper(II) complexes of novel tridentate ligands have been synthesized and characterized by spectroscopic methods and single crystal X-ray diffraction analysis. X-ray crystallographic studies reveal that the structure of mononuclear copper(II) complex with 2-[1-(methylamino-ethylimino)-ethyl]-phenol $[Cu(HAPMEN)(H_2O)_2]NO_3$ has distorted square pyramidal structure whereas the dinuclear complex with 2-[1-(proylamino-ethylimino)-methyl]-phenol $[Cu(SAPEN)]_2(ClO_4)_2$ has square planar geometry. Electrochemical behavior of these complexes was investigated by cyclic voltammetric studies. The complexes show quasi reversible cyclic voltammetric responses for the Cu(II)/Cu(I) couple. The binding properties of these complexes with calf-thymus DNA have been investigated by using absorption spectrophotometry. Mono nuclear complexes show unusually high binding affinity possible due to presence the labile aqua ligands. Cleavage activities of these complexes have been investigated on double stranded pBR 322 plasmid DNA by gel electrophoresis experiments under different conditions. Dinuclear complexes exhibit higher nuclease activity when compared with those of mononuclear complexes. The studies indicate that the cleavage of DNA takes place by oxidative mechanism in the presence of oxidant (H_2O_2).

1. Introduction

DNA is a significant cellular receptor, many chemicals bring to bear their antitumor effects by binding to DNA and by this means changes the replication of DNA and inhibits the growth of the tumor cells, which is the basis of designing new and more efficient antitumor drugs. During the last decade several transition metal complexes have been used as tools for understanding DNA structure, as agents for mediation of DNA cleavage or as chemotherapeutic agents. Metal complexes offer an opportunity to explore the effects of the effects of central metal atom, the ligands and the coordination geometries on the binding event. Moreover, their activity depends on the mode and affinity of their binding ability to the DNA strands [1–3]. A number of metal chelates have been used as agents for mediation of strand scission of duplex DNA, probes of DNA structure in solution and chemotherapeutic agents [4–6]. Platinum-based complexes had been in primary focus of research on chemotherapy agents [7–9]. The interests in this field recently have been shifted to non-platinum based agents in order to find different metal complexes [10–17]. Among these copper(II) complexes appear to be very promising agents for anticancer therapy having effective cytotoxic activities [18–21]. Copper is known essential metal. It is widely distributed in living cells and body. It is of interest to investigate DNA binding and cleavage activity of metal complexes of essential metals and thus attracted much attention.

Tridentate Schiff-bases are very efficient in coordinating with metal ions which prefer square-planar or square-pyramidal geometry. Such complexes are also important as models for copper proteins containing active metal sites [22–26]. A large number of mono and polynuclear complexes of imino-Schiff bases have been reported [27–31], but there are a few reports available in the literature on DNA binding and cleavage activities of such complexes [32].

In the light of the above and in continuation of our ongoing research on DNA binding and cleavage activities of transition metal complexes [32–37], herein we report the synthesis, crystal structures, DNA binding and cleavage activities of water soluble mono and dinuclear copper(II) complexes derived from tridentate Schiff base ligands.

* Corresponding author. Tel.: +91 8554224347.
E-mail address: khussainreddy@yahoo.co.in (K. Hussain Reddy).
[1] Address: Department of Chemistry, Government Degree College (Men), Anantapur 515001, Andhra Pradesh, India.

http://dx.doi.org/10.1016/j.ica.2014.01.010
0020-1693/

2. Experimental

2.1. Materials and methods

The reagents used in preparation of ligands were of reagent grade (Aldrich) and were used without further purification. Metal salts used in the synthesis of complexes were of reagent grade (Merck). Solvents used in the present study were distilled before use. Calf thymus DNA and plasmid pBR 322 were purchased from Genie Bio Labs, Bangalore, India. All other chemicals were of AR grade and used without further purification.

Caution! Although no problems were encountered in this work, perchlorate salts containing organic ligands are potentially explosive. They should be prepared in small quantities and handled with care.

2.1.1. Synthesis of ligands

5 mmol of 2-hydroxyacetophenone/salicylaldehyde (0.61/0.52 mL) dissolved in 30 mL of methanol were added to a methanolic solution (30 mL) of 5 mmol *N*-methylethylenediamine/*N*-propylethylenediamine (0.44/0.62 mL). The contents were refluxed over water bath for 1 h. The contents were then cooled and filtered. On evaporation of the solvent, 2-[1-(methylamino-ethylimino)-methyl]-phenol (SAMENH)/2-[1-(propylamino-ethylimino)-methyl]-phenol SAPENH/2-[1-(Methylamino-ethylimino)-ethyl]-phenol (HAPMENH)/2-[1-(propylamino-ethylimino)-ethyl]-phenol (HAPPENH) (Fig. 1) were yielded as reddish yellow coloured viscous liquids. The FT-IR spectra of ligands show vibrations at 3501–3510 cm^{-1} and 1615–1662 cm^{-1} corresponding to ν(NH) of secondary amine and azomethine ν(C=N) groups, respectively. The ligands were subsequently used in the preparation of metal complexes. ^{1}H NMR: SAPENH: δ(8.0) (singlet 1H), δ(7.45–6.76) (multiplet 4H), δ(5.0) (singlet 1H), δ(3.67) (triplet 2H), δ(3.67–2.91) (multiplet 4H), δ(2.0) (multiplet 1H), δ(2.55–2.15) (multiplet 4H) and δ(0.96) (triplet of triplet 3H) assigned to —CH=, aromatic ring protons, –O**H**, –C**H**$_2$–, –N**H**– and –NH–C**H**$_3$, respectively. HAPMENH: δ(7.15–6.78) (multiplet 4H), δ(5.56) (singlet 1H), δ(3.52–3.01) (multiplet 4H), δ(2.38) (multiplet 1H), δ(1.52) (singlet 3H) and δ(1.2) (doublet 3H) assigned to aromatic ring protons, –O**H**, –C**H**$_2$–, –N**H**–, –C**H**$_3$ and –NH–C**H**$_3$ respectively. For each complex the ligand is prepared separately and completely used for synthesis of one complex.

2.1.2. Synthesis of mononuclear copper(II) complex **(1)** 2-[1-(methylamino-ethylimino)-methyl]-phenol **[Cu(SAMEN)(H_2O)$_2$]NO_3**

To a methanolic solution (50 mL) of 5 mmol (1.2 g) copper(II)nitrate trihydrate, a methanolic solution (10 mL) of 5 mmol/0.885 g SAMEN was added and stirred magnetically for 30 min. A green coloured crystalline product was obtained which was filtered and washed with a minimum volume of methanol. Yield: 52% (0.881 g); Decomposition temperature: 274–276 °C. *Anal.* Calc. for $C_{10}H_{17}CuN_3O_6$: C, 35.42; H, 5.06; N, 12.42. Found: C, 35.45; H, 5.09; N, 12.48%.

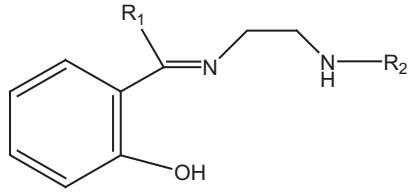

Ligand	R_1	R_2
SAMENH	H	CH_3
SAPENH	H	C_3H_7
HAPMENH	CH_3	CH_3
HAPPENH	CH_3	C_3H_7

Fig. 1. Structure of tridentate ligands.

2.1.3. Synthesis of mononuclear copper(II) complex **(2)** 2-[1-(proylamino-ethylimino)-methyl]-phenol **[Cu(SAPEN)(H_2O)$_2$]NO_3**

To a methanolic solution (50 mL) of 5 mmol (1.2 g) copper(II)nitrate trihydrate, a methanolic solution (10 mL) of 5 mmol/1.025 g SAPEN was added and stirred magnetically for 30 min. A green coloured product was obtained which was filtered and washed with a minimum volume of methanol. Yield: 59% (1.123 g); Decomposition temperature: 268–270 °C. *Anal.* Calc. for $C12H_{21}CuN_3O_6$: C, 39.29; H, 5.77; N, 11.45. Found: C, 39.22; H, 5.79; N, 11.43%.

2.1.4. Synthesis of synthesis of mononuclear copper(II) complex **(3)** 2-[1-(methylamino-ethylimino)-ethyl]-phenol **[Cu(HAPMEN)(H_2O)$_2$]NO_3**

To a methanolic solution (50 mL) of 5 mmol copper(II) nitrate trihydrate, a methanolic solution (10 mL) of 5 mmol/0.955 g HAPMEN was added and stirred magnetically for 30 min. A green coloured product was obtained which was filtered and washed with a minimum volume of methanol. Dark green single crystals suitable for X-ray analysis were grown by dissolving the product in methanol and slow dispersion of *n*-hexane. Yield: 49% (0.865 g); Decomposition temperature: 278–280 °C. *Anal.* Calc. for $C_{11}H_{19}CuN_3O_6$: C, 37.45; H, 5.43; N, 11.91. Found: C, 37.49; H, 5.42; N, 11.96%.

2.1.5. Synthesis of mononuclear copper(II) complex **(4)** 2-[1-(propylamino-ethylimino)-ethyl]-phenol **[Cu(HAPPEN)(H_2O)$_2$]NO_3**

To a methanolic solution (50 mL) of 5 mmol (1.2 g) copper(II)nitrate trihydrate, a methanolic solution (10 mL) of 5 mmol/1.095 g HAPPEN was added and stirred magnetically for 30 min. A green coloured product was obtained which was filtered and washed with a minimum volume of methanol. Yield: 52%; decomposition temperature: 265–267 °C (D). *Anal.* Calc. for $C_{13}H_{23}CuN_3O_6$: C, 40.99; H, 6.09; N, 11.03. Found: C, 40.92; H, 6.01; N, 11.07%.

2.1.6. Synthesis of dinuclear copper(II) complex **(5)** 2-[1-(methylamino-ethylimino)-methyl]-phenol **[Cu(SAMEN)]$_2$(ClO_4)$_2$**

To a methanolic solution (50 mL) of 5 mmol (1.853 g) $Cu(ClO_4)_2\cdot 6H_2O$, a methanolic solution (10 mL) of 5 mmol/0.885 g SAMEN was added and stirred magnetically for 30 min. Triethylamine (5 mmol, 0.85 mL) was added drop wise to the contents with constant stirring. A green coloured product was obtained which was filtered and washed with a minimum volume of methanol. Yield: 59% (2.006 g); decomposition temperature: 255–257 °C. *Anal.* Calc. for $C_{20}H_{26}Cl_2Cu_2N_4O_{10}$: C, 35.41; H, 3.94; N, 8.23. Found: C, 35.27; H, 3.82; N, 7.97%.

2.1.7. Synthesis of dinuclear copper(II) complex **(6)** 2-[1-(proylamino-ethylimino)-methyl]-phenol **[Cu(SAPEN)]$_2$(ClO_4)$_2$**

To a methanolic solution (50 mL) of 5 mmol $Cu(ClO_4)_2\cdot 6H_2O$, a methanolic solution (10 mL) of 5 mmol/1.025 g SAPEN was added and stirred magnetically for 30 min. Triethylamine (5 mmol, 0.85 mL) was added drop wise to the contents with constant stirring. A green coloured product was obtained which was filtered and washed with a minimum volume of methanol. Dark green coloured hexagonal single crystals suitable for X-ray analysis were grown by dissolving the product in acetonitrile solution and slow dispersion of *n*-hexane. Yield: 54% (1.98 g); decomposition tem-

perature: 242–244 °C. *Anal.* Calc. for $C_{24}H_{34}Cl_2Cu_2N_4O_{10}$: C, 39.14; H, 4.65; N, 7.61. Found: C, 39.26; H, 4.58; N, 7.66%.

2.1.8. Synthesis of dinuclear copper(II) complex ***(7)*** *2-[1-(methylamino-ethylimino)-ethyl]-phenol* ***[Cu(HAPMEN)]$_2$(ClO$_4$)$_2$***

To a methanolic solution (50 mL) of 5 mmol (1.853 g) $Cu(ClO_4)_2\cdot 6H_2O$, a methanolic solution (10 mL) of 5 mmol/0.955 g HAPMEN was added and stirred magnetically for 30 min. Triethylamine (5 mmol, 0.85 mL) was added drop wise to the contents with constant stirring. A green coloured product was obtained which was filtered and washed with a minimum volume of methanol. Yield: 49% (1.734 g); decomposition temperature: 270–272 °C. *Anal.* Calc. for $C_{22}H_{30}Cl_2Cu_2N_4O_{10}$: C, 37.28; H, 4.27; N, 7.91. Found: C, 37.46; H, 4.23; N, 7.75%.

2.1.9. Synthesis of dinuclear copper(II) complex ***(8)*** *2-[1-(propylamino-ethylimino)-ethyl]-phenol* ***[Cu(HAPPEN)]$_2$(ClO$_4$)$_2$***

To a methanolic solution (50 mL) of 5 mmol (1.85 g) $Cu(ClO_4)_2\cdot 6H_2O$, a methanolic solution (10 mL) of 5 mmol/1.095 g HAPPEN was added and stirred magnetically for 30 min. Triethylamine (5 mmol, 0.85 mL) was added drop wise to the contents with constant stirring. A green coloured product was obtained which was filtered and washed with a minimum volume of methanol. Yield: 52% (1.986 g); decomposition temperature: 185–187 °C. *Anal.* Calc. for $C_{26}H_{38}Cl_2Cu_2N_4O_{10}$: C, 40.83; H, 4.97; N, 7.34. Found: C, 40.89; H, 4.87; N, 7.45%.

2.2. Physical measurements

Infrared spectra in KBr disc were recorded in the range 4000–400 cm^{-1} with a Perkin-Elmer spectrum 100 spectrometer. Electronic spectra were recorded in *N*,*N*-dimethylformamide with a Perkin-Elmer UV Lamda-50 spectrophotometer. Elemental analyses were carried out on a Heraeus Vario EL III Carlo Erba 1108 instrument. Magnetic measurements of all the complexes at 298 K in the present study are obtained on a Faraday's magnetic susceptibility balance (Sherwood Scientific, Cambridge, UK). High purity copper sulfate pentahydrate was used as a standard. The conductance measurements at 298 ± 2 K in water were carried out on CM model 162 Conductivity cell (ELICO). ESR spectra were recorded in solid state and in solution state at 298 K and at liquid nitrogen temperature (L.N.T) on Varian E-112 spectrometer with 100 kHz field modulation. Temperature dependent magnetic susceptibility measurements were carried out with a Lakeshore VSM 7410 magnetometer, at SAIF, IIT-M, Chennai, under an applied magnetic field of 5000 Oe. Magnetic data were corrected for diamagnetic contributions estimated from Pascal tables and for the sample holder contributions of a sample holder. Cyclic voltammetry was performed with a CH Instruments 660C Electrochemical Analyzer and a conventional time electrode, Ag/AgCl reference electrode, glassy carbon working electrode and platinum counter electrode. Nitrogen was used as purge gas and all solutions were prepared in water containing 0.1 M concentration in tetrabutylammonium hexafloro phosphate ($TBAPF_6$).

2.3. X-ray crystallography

Crystal data were collected by using the Enraf Nonius CAD4-MV31 single crystal X-ray diffractometer, Indian Institute of Technology-Madras, Chennai. Enraf Nonius CAD4-MV31 single crystal X-ray diffractometer is a fully automated four circle instrument controlled by a computer. It consists of an FR 590 generator, a goniometer, CAD4F interface and a microVAX3100 equipped with a printer and plotter. The detector is a scintillation counter. A single crystal is mounted on a thin glass fiber fixed on the goniometer head. The unit cell dimensions and orientation matrix are determined using 25 reflections and then the intensity data of a given set of reflections are collected automatically by the computer. An IBM compatible PC/AT 486 is attached to micro VAX facilitating the data transfer onto a DOS floppy of 5.25″ or 3.5″. Maximum X-ray power is 40 mA × 50 kV.

The data collected was reduced using SAINT program [38]. The trial structure was obtained by direct method [39] using SHELXS-86, which revealed the position of all non-hydrogen atoms and refined by full-matrix least squares on F^2 (SHELXS-97) [40] and graphic tool was DIAMOND for windows [41]. All non-hydrogen atoms were refined anisotropically, while the hydrogen atoms were treated with a mixture of independent and constrained refinements.

2.4. DNA binding experiments

The interaction of the complexes with DNA was carried out in tris-buffer. Solution of calf thymus-DNA (CT-DNA) in (0.5 mM NaCl/5 mM Tris–HCl; pH 7.0) buffer gave absorbance ratio at 260 and 280 nm of 1.89 indicating that the DNA was sufficiently free of proteins. The DNA concentration per nucleotide was determined by absorption coefficient (6600 $dm^3\ mol^{-1}\ cm^{-1}$) at 260 nm. Stock solutions stored at 4 °C were used after no more than four days. The electronic spectra of metal complexes in aqueous solutions were monitored in the absence and presence of CT-DNA. Absorption titrations were performed by maintaining the metal complex concentration 20×10^{-6} M and varying the nucleic acid concentration (0–26.4×10^{-6} M). The ratio of r = [complex]/[DNA] values vary from 6.51 to 0.72. Absorption spectra were recorded after each successive addition of DNA solution.

2.5. DNA cleavage experiments

The extent of cleavage of DNA mono and dinuclear copper(II) complexes was monitored using agarose gel electrophoresis with pBR 322 DNA. After incubation for 30 min at 37 °C, the samples were added to the loading buffer containing 0.25% bromophenol blue + 0.25% xylene cyanol + 30% glycerol, and solutions were loaded on 0.8% agarose gel containing 100 μg of ethidium bromide. Electrophoresis was performed at 75 V in TBE buffer until the bromophenol blue reached to 3/4 of the gel. Bands were visualized by UV Transilluminator and photographed. The efficiency of DNA cleavage was measured by determining the ability of the complex to form open circular (OC) or nicked circular (NC) DNA from its supercoiled (SC) form. The reactions were carried out under different conditions.

3. Results and discussion

Reactions of tridentate ligands with $Cu(NO_3)\cdot 3H_2O$ yielded in the formation of mononuclear complexes (complexes **1**–**4**) whereas the same ligands in presence of triethylamine react with $Cu(ClO_4)_2\cdot 6H_2O$ yielding in the formation of dinuclear copper(II) complexes (complexes **5**–**8**). All the complexes are dark green coloured and freely soluble in water and many organic solvents. Molar conductivity values (58–69 $\Omega^{-1}\ cm^2\ mol^{-1}$ for complexes **1**–**4** and 124–178 $\Omega^{-1}\ cm^2\ mol^{-1}$ for complexes **5**–**8**) suggest that mononuclear complexes are 1:1 electrolytic, whereas the dinuclear metal complexes are 1:2 electrolytic [42]. Magnetic susceptibility measurements reveal that complexes **1**–**4** (μ_{eff} = 1.78–1.90 BM) are monomeric and there are no metal–metal interactions [43]. The magnetic moment values of complexes **5**–**8** are found to be in the range of 1.14–1.26 BM which are sub-normal to spin only value. The data reveal that these complexes are dimeric and there are strong metal–metal interactions between the two copper centers.

Table 1
Spin Hamiltanian and orbital reduction parameters for the copper(II) complexes.

Complex	In solid state at 77 K				In solution state at 77 K											
	$g_{\|}$	$g_{\perp}$	g_{av}	G	$g_{\|}$	$g_{\perp}$	g_{av}	G	λ	$K_{\|}$	$K_{\perp}$	$A_{\|}$ (cm^{-1})	$A_{\perp}$ (cm^{-1})	A_{av} (cm^{-1})	$g_{\|}/A_{\|}$	α^2
Complex **1**	2.046	2.011	2.023	4.752	2.144	2.030	2.068	5.046	283	1.020	0.908	0.0105	0.0023	0.0050	204	0.097
Complex **2**	2.153	2.040	2.077	4.007	2.180	2.043	2.088	4.373	365	1.001	0.959	0.0103	0.0023	0.0049	211	0.052
Complex **3**	2.207	2.021	2.040	4.117	2.197	2.050	2.099	4.098	408	0.991	0.980	0.0098	0.0017	0.0044	224	0.018
Complex **4**	2.213	2.036	2.070	4.011	2.216	2.055	2.109	4.005	441	0.988	0.989	0.0096	0.0014	0.0041	230	0.010
Complex **5**	2.066	2.049	2.055	1.344	2.204	2.098	2.133	2.107	541	0.871	1.429	0.0134	0.0062	0.0086	164	0.523
Complex **6**	2.079	2.056	2.064	1.428	2.127	2.059	2.081	2.199	331	0.874	1.179	0.0072	0.0051	0.0058	295	0.391
Complex **7**	2.070	2.057	2.062	1.247	2.198	2.082	2.120	2.496	494	0.901	1.147	0.0131	0.0060	0.0084	167	0.635
Complex **8**	2.080	2.054	2.061	1.506	2.126	2.054	2.078	2.392	319	0.890	1.151	0.0065	0.0031	0.0043	327	0.366

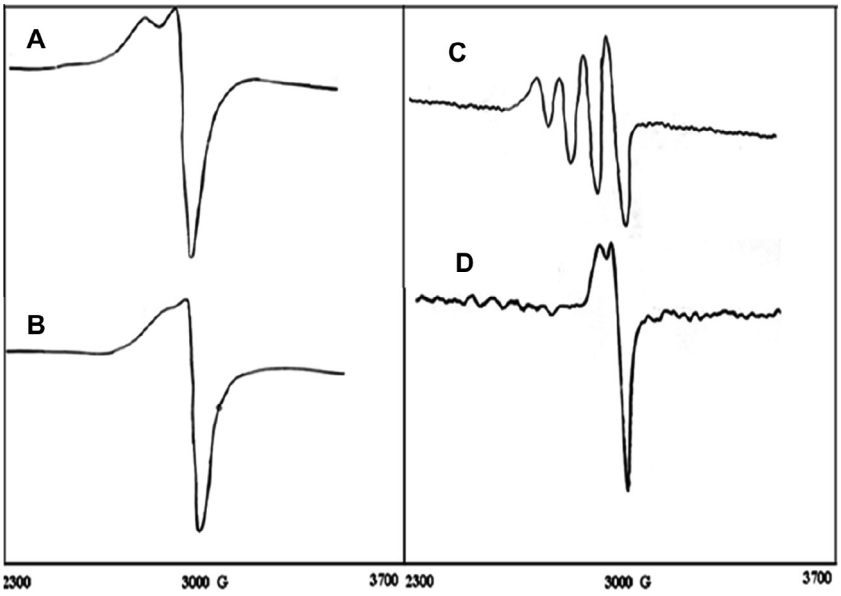

Fig. 2. (A) X-band powder ESR spectra of $[Cu(HAPMEN(H_2O)_2]NO_3$ at 300 K, (B) at LNT, (C) in DMF solution at 300 K and (D) at LNT in DMF solution.

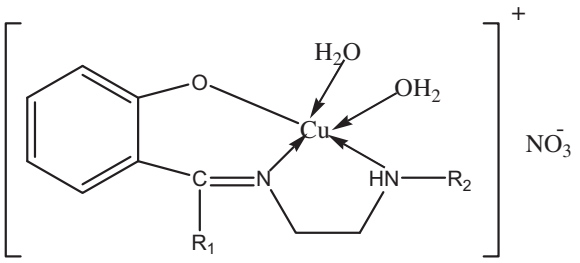

Where $R_1 = H/CH_3$ and $R_2 = CH_3/C_3H_7$

Fig. 3. Suggested structure for mononuclear copper(II) complexes **1–4**.

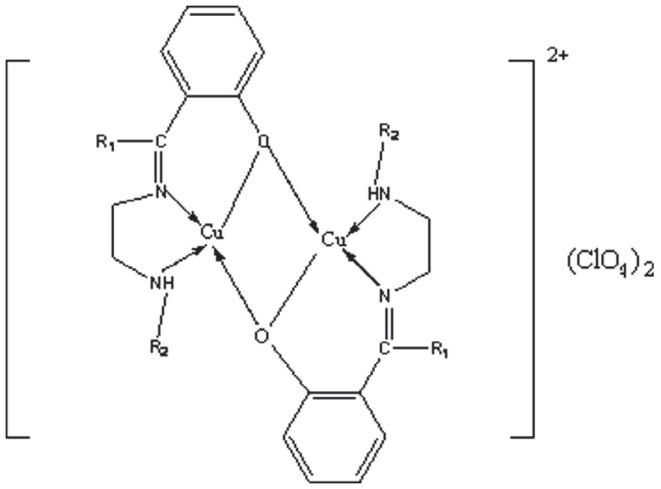

Where $R_1 = H/CH_3$ and $R_2 = CH_3/ C_3H_7$

Fig. 4. Suggested structure for dinuclear copper(II) complexes **5–8**.

3.1. Spectral characterization

The electronic spectral data of copper(II) complexes are recorded in water and in dimethylformamide (DMF). In aqueous solutions electronic spectra of complexes **1–4** show medium bands in the region 27244–27984 cm^{-1} are due to metal to ligand charge transfer transition (MLCT). Bands observed in the region 12484–12285 cm^{-1} followed by a band in the regions 16130–16548 cm^{-1} are attributed due to d-d transitions suggest square pyramidal geometry around Cu(II) atom [43–45]. In DMF the absorption bands are shifted to higher wavelengths (bathochromic shift, $\Delta\lambda$ = 9–14 nm) suggesting the involvement of solvent molecules in coordination. In aqueous solution the dinuclear complexes **5–8** show medium intensity bands in the region 27548–28818 cm^{-1} is due to metal to ligand charge transfer transition (MLCT). Whereas one broad band observed in the region 16447–16722 cm^{-1} (λ = 598–608 nm) is assigned to d–d transition. In DMF the absorption bands are shifted to higher

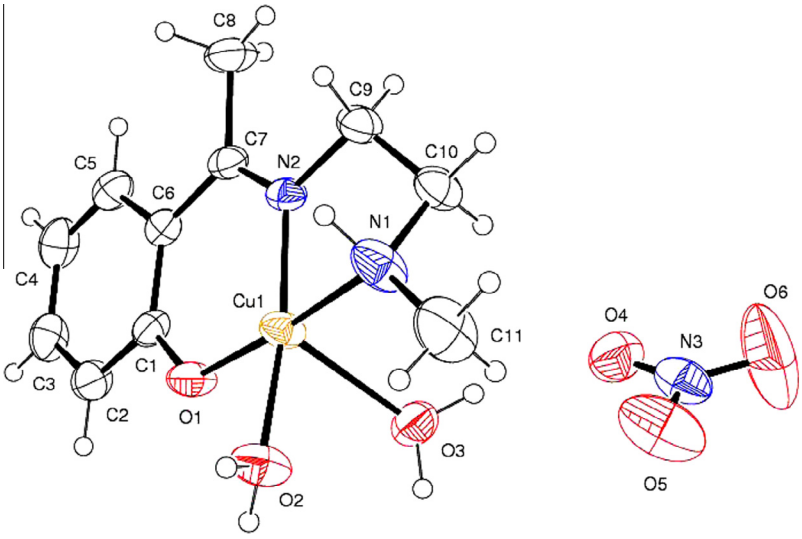

Fig. 5. ORTEP view of complex 3.

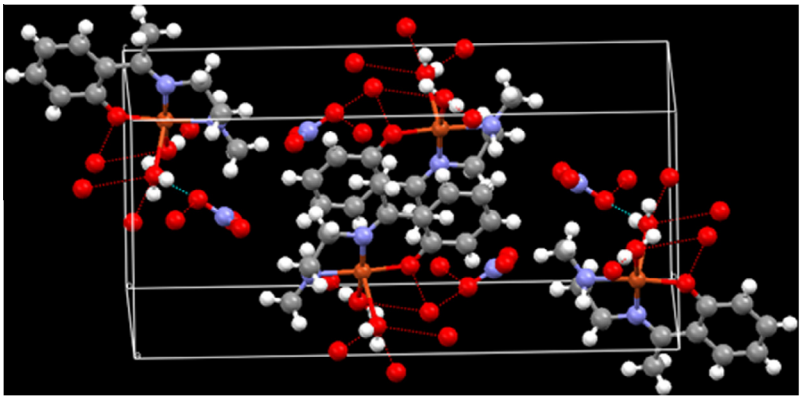

Fig. 6. Close packing diagram of complex 3.

wavelengths suggesting the involvement of solvent molecules in coordination. Bathochromic shift of absorption bands in d–d transition region is $\Delta\lambda$ = 6–13 nm. The electronic spectra of these complexes display weak d–d bands in the low intensity 16233–16393 cm^{-1} region are assigned to $^2E_g \rightarrow {}^2T_{2g}$ electronic transition in favor of octahedral structure in DMF medium. Six coordination for copper(II) is facilitated by axial coordination of DMF solvent molecules.

This band is shifted to lower wave number in IR spectra of all the complexes suggesting the participation of azomethine nitrogen atom in coordination with metal atom.

The FT-IR spectra of ligands show vibrations at 3501–3510 cm^{-1} and 1615–1662 cm^{-1} corresponding to ν(NH) of secondary amine and azomethine ν(C=N) groups respectively. The FT-IR spectra of complexes **1**–**4** show vibrations in the regions 3416–3454, 3100–3200 and 1610–1635 cm^{-1} corresponding to ν(NH) of secondary amine, ν(OH) of coordinated water molecule and azomethine ν(C=N) groups respectively. The bands shifted to lower wave number in IR spectra of all the complexes suggest the participation of azomethine nitrogen atom in coordination with metal atom. The sharp bands observed in the region 1360–1338 cm^{-1} are due to the non-coordinated nitrate ions present outside the coordination sphere [46]. FT-IR spectra of complexes **5**–**8** display vibrations in the regions 3413–3436 cm^{-1} and 1584–1637 cm^{-1} corresponding to ν(NH) and ν(C=N), respectively. When ClO_4^- ions are considered, ν_3 mode bands in the region 1077–1115 cm^{-1} are slightly broadened, but the ν_4 bands in the region 624–626 cm^{-1} is the devoid of any splitting and is consistent with the IR normal modes for a T_d symmetry, suggesting that these anions [ClO_4^-] are not coordinated to the metal atom [47].

3.1.1. ESR spectral studies

The spin Hamiltonian and orbital reduction parameters of complexes **1**–**8** are shown in Table 1. Typical X-band ESR spectra of [Cu(HAPMEN)$(H_2O)_2$]NO_3 (complex **3**) are shown in Fig. 2. The $g_{\|}$ and $g_{\perp}$ values are computed from the spectrum using (TCNE) free radical as '*g*' marker. From the observed values of complexes **1**–**4** at 300 K and 77 K in solid state spectrum, it is clear that $g_{\|} > g_{\perp} > 2.00$ which suggest the fact that the unpaired electron lies predominantly in the $d_{x^2-y^2}$ orbital [48] characteristic of square pyramidal geometry in copper(II) complexes [45]. For ESR spectra at 77 and 300 K, the '*G*' values are found to be more than 4, which suggest that there are no interactions between copper(II) ions in the solid state or in solution state. The solution EPR spectra show four-hyperfine signals at 300 K, which were not observed in DMF at 77 K. The spin–orbit coupling constant, λ value of the complexes calculated using the relations, $g_{av} = 1/3[g_{\|} + 2\,g_{\perp}]$ and $g_{av} = 2(1 - 2\lambda/10Dq)$, is less than the free Cu(II) ion (−832 cm^{-1}) which

Table 2
Crystal data and structure refinement for $[Cu(HAPMEN)(H_2O)_2]NO_3$ and $[Cu(SAPEN)]_2(ClO_4)_2$.

	$[Cu(HAPMEN)(H_2O)_2]NO_3$	$[Cu(SAPEN)]_2(ClO_4)_2$
Empirical formula	$C_{11}H_{19}CuN_3O_6$	$C_{24}H_{34}Cl_2Cu_2N_4O_{10}$
Formula weight	352.83	736.53
T (K)	293(2)	293(2)
Wavelength (Mo Kα) (Å)	0.71073	0.71073
Crystal system	monoclinic	monoclinic
Space group	$P21/n$	$P21/c$
Unit cell dimensions		
a (Å)	7.874(5)	11.9790(5)
b (Å)	20.908(4)	14.7940(5)
c (Å)	9.119(2)	17.0060(6)
β (°)	107.324(5)	102.0400(10)
V (Å^3)	1433.2(10)	2947.46(19)
Z	4	4
Calculated density, ρ (Mg m^{-3})	1.635	1.660
Absorption coefficient μ (mm^{-1})	1.555	1.685
$F(000)$	732	1512
Crystal size (mm)	0.30 × 0.20 × 0.20	0.20 × 0.20 × 0.15
θ Range for data collection (°)	2.53–24.99	2.22–25.00
Limiting indices	$-9 \leqslant h \leqslant 9$, $-23 \leqslant k \leqslant 24$, $-10 \leqslant l \leqslant 10$	$-14 \leqslant h \leqslant 14$, $-17 \leqslant k \leqslant 17$, $-20 \leqslant l \leqslant 20$
Reflections collected	13991	26437
Unique reflections (R_{int})	2513 (0.0236)	5184 (0.0304)
Completeness to θ (%)	24.99–99.8	25.00–100.0
Absorption correction	semi-empirical from equivalents	semi-empirical from equivalents
Maximum and minimum transmission	0.7512 and 0.6462	0.7942 and 0.7190
Refinement method	full-matrix least-squares on F^2	full-matrix least-squares on F^2
Data/restraints/parameters	2513/8/212	5184/70/426
Goodness-of-fit (GOF) on F^2	1.181	1.039
Final R indices [$I > 2\sigma(I)$]	$R_1 = 0.0465$[a], $wR_2 = 0.1061$[b,c]	$R_1 = 0.0281$, $wR_2 = 0.0694$
R indices (all data)	$R_1 = 0.0572$[a], $wR_2 = 0.1362$[b,c]	$R_1 = 0.0372$, $wR_2 = 0.0755$
Largest difference in peak and hole (e A^{-3})	0.685 and −0.400	0.621 and −0.289

[a] $R_1 = \sum(|F_O| - |F_C|)/\sum|F_O|$.
[b] $wR_2 = \{\sum[w(F_O^2 - F_C^2)^2]/\sum[w(F_O^2)^2]\}^{1/2}$.
[c] $w = 1/[\sigma^2(F_O^2)+(aP)^2 + bP]$ with $P = [F_o^2 + 2F_c^2]/3$, $a = 0.0612$ and $b = 0.24$.

Table 3
Hydrogen bond geometry for $[Cu(HAPMEN)(H_2O)_2]NO_3$ [Å and °].

D–H···A	d(D–H)	d(H···A)	d(D···A)	∠(DHA)
O(2)-H(2B)...O(3)#1	0.875(19)	2.12(4)	2.871(5)	144(6)
O(2)-H(2A)...O(4)#2	0.875(19)	2.54(5)	3.169(5)	129(5)
O(2)-H(2A)...O(4)#2	0.895(19)	1.92(3)	2.799(6)	165(5)
O(2)-H(2A)...O(6)#2	0.895(19)	2.47(5)	3.162(8)	135(5)
O(2)-H(2A)...N(3)#2	0.895(19)	2.54(3)	3.384(6)	157(6)
O(3)-H(3A)...O(4)	0.880(19)	1.95(3)	2.812(6)	165(5)
O(3)-H(3B)...O(1)#1	0.890(2)	1.98(3)	2.808(5)	154(6)

Symmetry transformations used to generate equivalent atoms: #1 $-x+2$, $-y$, $-z+3$; #2 $x+1$, y, z.

supports the covalent nature of M–L bond in the complexes [49]. The greater value of $g_{\|}$ compared to $g_{\perp}$ proposes a distorted square pyramidal structure and rules out the possibility of a trigonal bipyramidal structure which is expected to have $g_{\perp} > g_{\|}$ [50,51]. Increasing steric hindrance caused by bulky ligands results in the lowest $A_{\|}$ and highest $g_{\|}$ values, which in turn reflects in square pyramidal distortion of copper(II) geometries. As the bulkiness increases, an increased distortion in square pyramidal structure is observed which is reflected in the values of $g_{\|}/A_{\|}$ [52]. Also, the observed $g_{\|}$ values of less than 2.3 provide evidence for the covalent character of bonding between Cu(II) ion and the ligand [53]. The observed $K_{\|} > K_{\perp}$ relation for mononuclear copper(II) complexes indicates the presence of out-of-plane π-bonding [50]. The in-plane bonding parameter α^2 values are calculated using the relation $\alpha^2 = -(A_{\|}/0.036) + (g_{\|} - 2.0023) + 3/7\,(g_{\perp} - 2.0023) + 0.04$.

For ESR spectra of complexes **5**–**8** at 77 and 300 K, the 'G' values are found to be less than 4 suggesting metal–metal interactions between copper(II) ions in the solid state which further supports the dinuclear nature of the complexes. The observed $K_{\|} < K_{\perp}$ relation

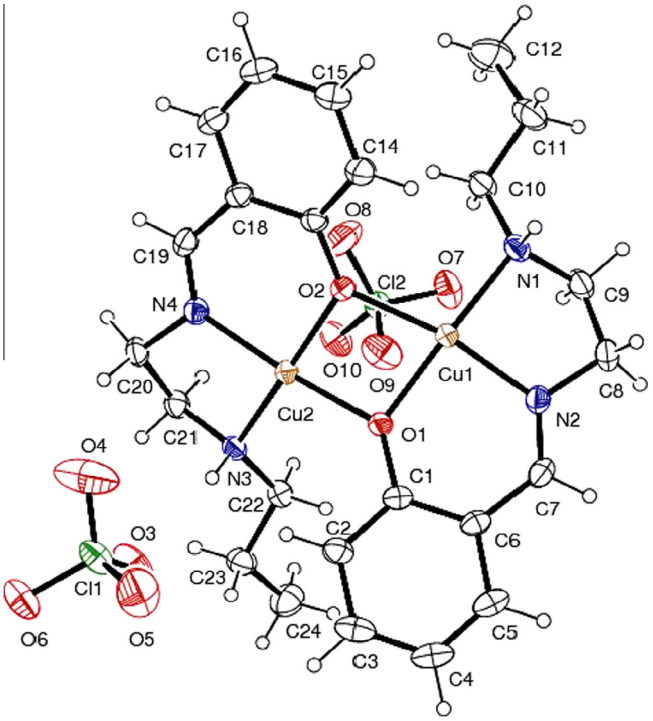

Fig. 7. ORTEP view of the complex **6**. Ellipsoids drawn at 50% probability level.

for dinuclear copper(II) complexes indicates the presence of in-plane π-bonding [50]. Increasing steric hindrance caused by bulky ligands results in the lowest $A_{\|}$ and highest $g_{\|}$ values.

Table 4
Selected bond lengths (Å) and bond angles (°) for $[Cu(HAPMEN)(H_2O)_2]NO_3$.

Bond lengths (Å)		Bond angles (°)	
N(1)–Cu(1)	1.999(4)	C(11)–N(1)–Cu(1)	122.0(4)
N(1)–H(1)	0.97(2)	C(10)–N(1)–Cu(1)	103.3(3)
N(2)–Cu(1)	1.955(3)	C(7)–N(2)–Cu(1)	127.7(3)
N(3)–O(5)	1.178(6)	C(9)–N(2)–Cu(1)	111.0(3)
N(3)–O(6)	1.183(6)	C(1)–O(1)–Cu(1)	127.0(3)
N(3)–O(4)	1.241(6)	Cu(1)–O(2)–H(2B)	118(4)
O(1)–Cu(1)	1.878(3)	Cu(1)–O(2)–H(2A)	121(4)
O(2)–Cu(1)	2.006(3)	Cu(1)–O(3)–H(3A)	118(4)
O(2)–H(2B)	0.875(19)	Cu(1)–O(3)–H(3B)	115(4)
O(2)–H(2A)	0.895(19)	O(1)–Cu(1)–N(2)	93.25(13)
O(3)–Cu(1)	2.417(4)	O(1)–Cu(1)–N(1)	175.89(18)
O(3)–H(3A)	0.880(19)	N(2)–Cu(1)–N(1)	84.74(15)
O(3)–H(3B)	0.89(2)	O(1)–Cu(1)–O(2)	88.27(13)
		N(2)–Cu(1)–O(2)	169.88(15)
		N(1)–Cu(1)–O(2)	93.09(15)
		O(1)–Cu(1)–O(3)	88.71(13)
		N(2)–Cu(1)–O(3)	105.44(14)
		N(1)–Cu(1)–O(3)	95.27(18)
		O(2)–Cu(1)–O(3)	84.59(16)

Based on physico-chemical and spectral data, structures of mono and dinuclear complexes are given in Figs. 3 and 4.

3.2. Description of crystal structures

3.2.1. Description of crystal structure of $[Cu(HAPMEN)(H_2O)_2]NO_3$ (complex **3**)

The complex crystallizes in monoclinic, space group $P2_1/n$. Crystal data and structure refinements are shown in Table 2. The ORTEP view is shown in Fig. 5 together with the numbering scheme in the metal coordination sphere. The molecule contains a five coordinated Cu(II) atom, while the basal plane is occupied by three donor atoms O(1), N(1), N(2) of the tridentate ligand together with two oxygen atoms O(2) and O(3) of the coordinated water molecules. The axial Cu(1)–O(3) bond distance of 2.417(4) Å is larger than the basal Cu(1)–O(1) and Cu(1)–O(2) bond distances of 1.878(3) and 2.006(3) Å, respectively. This indicates distorted square-pyramidal geometry of mononuclear complex [54,55]. Close packing diagram of $[Cu(HAPMEN)(H_2O)_2]NO_3$ is shown in Fig. 6. Geometric details describing the intermolecular O(3)–H(3A)···O(4) hydrogen bond in the complex: H(3A)···1.95(3) Å, O(3)···O(4) = 2.812(6) Å with angle at H(2B) = 165(5). Intermolecular interactions operating in the crystal structure of $[Cu(HAPMEN)(H_2O)_2]NO_3$: O(2)–H(2B)···$O(3)^{\#1}$ = 2.14(4) Å; O(2)–O(3) = 2.871(5) Å with angle at H(2B) = 144(6) for symmetry operation #1 $-x+2, -y, -z+3$; O(3)–H(3B)···$O(1)^{\#1}$ = 1.98(4) Å; O(3)–O(1) = 2.808(5) Å with angle at H(2B) = 154(6) for symmetry operation #1 $-x+2, -y, -z+3$ and O(2)–H(2A)···$O(4)^{\#2}$ = 2.54(5) Å; O(2)···O(4) = 3.168(5) Å with angle at H(2)A = 129(5)° for #2 $x+1, y, z$. Hydrogen bonding data are listed in Table 3. Selected bond lengths and bond angles are summarized in Table 4.

3.2.2. Description of crystal structure of ***[Cu(SAPEN)]$_2$(ClO$_4$)$_2$*** (complex ***6***)

The X-ray crystallographic analysis reveals that complex **6** is a binuclear entity with the formula $C_{24}H_{34}Cl_2Cu_2N_4O_{10}$. The complex crystallizes in monoclinic, space group $P21/c$. Crystal data and structure refinements are shown in Table 2. The structure is shown

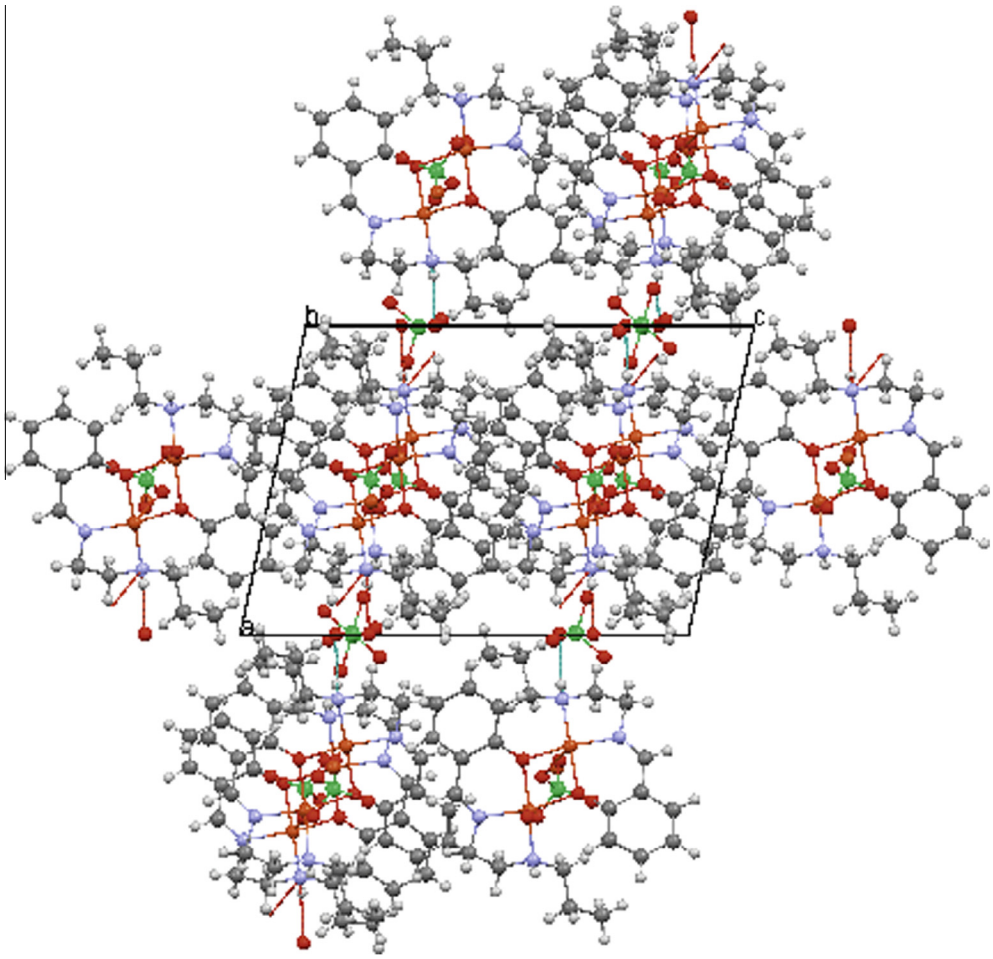

Fig. 8. Close packing diagram of complex **6**.

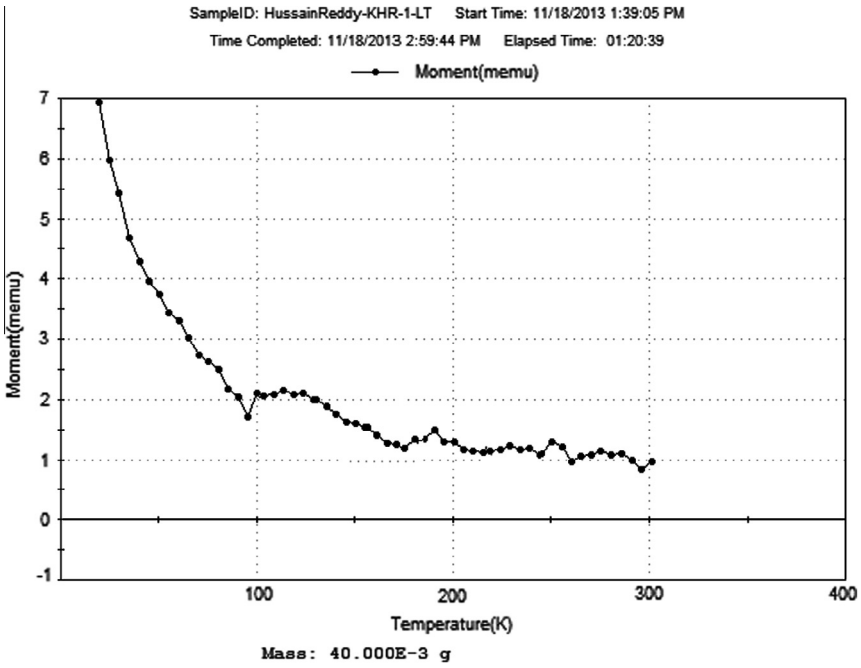

Fig. 9. ZFC magnetization curve of complex **6**.

Table 5
Selected bond lengths (Å) and bond angles (°) for $[Cu(SAPEN)]_2\ 2ClO_4$.

Bond lengths (Å)		Bond angles (°)	
N(1)–Cu(1)	2.004(2)	C(10)–N(1)–Cu(1)	117.52(16)
N(2)–Cu(1)	1.931(2)	Cu(1)–N(1)–H(1A)	107.9(19)
N(3)–Cu(2)	2.005(2)	C(7)–N(2)–Cu(1)	126.6(2)
N(4)–Cu(2)	1.923(2)	C(8)–N(2)–Cu(1)	112.55(18)
O(1)–Cu(1)	1.9299(17)	C(21)–N(3)–Cu(2)	104.63(16)
O(1)–Cu(2)	1.9420(16)	C(22)–N(3)–Cu(2)	118.66(16)
O(2)–Cu(2)	1.9435(17)	Cu(2)–N(3)–H(3A)	106.6(19)
O(2)–Cu(1)	1.9655(16)	C(19)–N(4)–Cu(2)	126.62(18)
Cu(1)–Cu(2)	2.9278(4)	C(20)–N(4)–Cu(2)	111.97(16)
		C(1)–O(1)–Cu(1)	127.55(16)
		C(1)–O(1)–Cu(2)	134.09(16)
		Cu(1)–O(1)–Cu(2)	98.25(7)
		C(13)–O(2)–Cu(2)	128.10(15)
		C(13)–O(2)–Cu(1)	134.88(16)
		Cu(2)–O(2)–Cu(1)	97.00(7)
		O(1)–Cu(1)–N(2)	90.88(8)
		O(1)–Cu(1)–O(2)	78.04(7)
		N(2)–Cu(1)–O(2)	168.91(8)
		O(1)–Cu(1)–N(1)	163.58(9)
		N(2)–Cu(1)–N(1)	85.82(9)
		O(2)–Cu(1)–N(1)	104.87(8)
		O(1)–Cu(1)–Cu(2)	41.03(5)
		N(2)–Cu(1)–Cu(2)	128.42(7)
		O(2)–Cu(1)–Cu(2)	41.21(5)
		N(1)–Cu(1)–Cu(2)	133.79(7)
		N(4)–Cu(2)–O(1)	167.01(8)
		N(4)–Cu(2)–O(2)	92.33(8)
		O(1)–Cu(2)–O(2)	78.28(7)
		N(4)–Cu(2)–N(3)	86.31(9)
		O(1)–Cu(2)–N(3)	104.20(8)
		O(2)–Cu(2)–N(3)	172.15(8)
		N(4)–Cu(2)–Cu(1)	132.85(7)
		O(1)–Cu(2)–Cu(1)	40.72(5)
		O(2)–Cu(2)–Cu(1)	41.78(5)
		N(3)–Cu(2)–Cu(1)	137.30(6)

in Fig. 7 together with the numbering scheme in the metal coordination sphere. Close packing diagram of the complex is shown in Fig. 8.

Table 6
Hydrogen bonds for $[Cu(SAPEN)]_2\ 2ClO_4$ (Å and °).

D–H···A	*d*(D–H)	*d*(H···A)	*d*(D···A)	∠(DHA)
N(1)–H(1A)···O(6′)#1	0.835(17)	2.26(3)	3.082(18)	170(3)
N(1)–H(1A)···O(6)#	0.835(17)	2.28(2)	3.084(6)	162(2)
N(3)–H(3A)···O(3)	0.825(17)	2.233(19)	3.037(6)	165(3)
N(3)–H(3A)···O(4′)	0.825(17)	2.34(3)	3.03(2)	141(3)

Symmetry transformations used to generate equivalent atoms: #1 *x* + 1, *y*, *z*.

Dinuclear cation of the complex comprises two [Cu(SAPEN)] subunits, which are interconnected through two oxygen bridges afforded by the oxygen atoms of the ligands. The copper center has square-planar geometry with the coordination of two nitrogen atoms and one oxygen atom from the tridentate ligand while the oxygen atoms of the ligands forming bridges in between the two Cu atoms. In the cation $[(CuSAPEN)]_2^{2+}$, the average bond lengths in the square planar coordination sphere are Cu–N(amino) 2.0045 Å, Cu–N(imino) 1.927 Å, Cu–O(ligand) 1.9367 Å, and Cu–O(axial) 1.9537 Å, respectively. The axial Cu–O bonds are longer than those of equatorial oxygen atoms of the ligands. The distance between the two copper atoms is 2.9278 Å and the Cu–O–Cu bridging angles are 98.25(7)° and 97(7)°. The sums of the bond angles around the bridging oxygen atoms are 359.89° and 359.98°, indicating that these bonds are essentially planar. Selected bond lengths and selected bond angles are presented in Table 5. Hydrogen bonding data are listed in Table 6.

There are some other reports in the literature [56,57], in which similar type of crystal structures derived from same type of ligands are found. In both the reports dinuclear copper(II) complexes were found, but the difference is that the Cu(II) centres are five-coordinated and have square-pyramidal geometry. Moreover in both the reports the bridging oxygen atoms are afforded by H_2O ligands. In present study we report four coordinated complexes with square planar geometry around the Cu(II) moieties and the bridging oxygen atoms are from phenolic moieties.

The single crystal X-ray diffraction analysis confirms the structures suggested in Figs. 3 and 4 based on physico-chemical and spectral analysis.

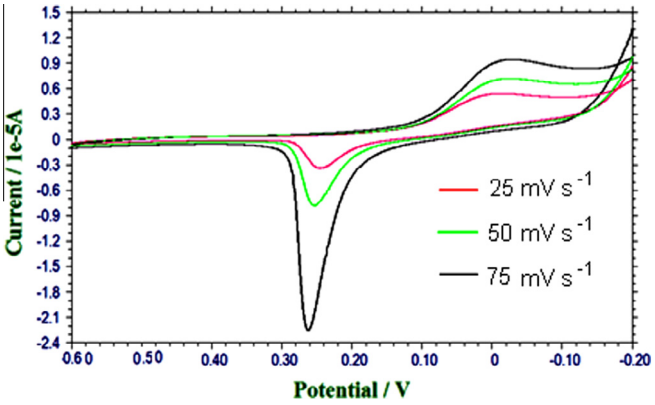

Fig. 10. Cyclic voltammetric profiles of complex 4 at different scan rates 25, 50 and 75 mV s^{-1}.

3.3. Magnetic properties

The temperature dependent molar magnetic susceptibilities, χ_M for complexes **3** and **6** were measured in the temperature range 20–300 K. At 300 K the magnetic moment value for complex **3** is in good agreement with the value expected. For complex **6** the value of χ_M at 300 K is 0.99 emu which is subnormal to spin only value. This value increases ($\chi_M \times T$ value decreases) slightly as the temperature is lowered, and below 100 K it increases very rapidly. This is a characteristic magnetic behavior of an antiferromagnetically coupled dimer. The ZFC magnetization curve of complex **6** as a function of temperature is shown in Fig. 9. To estimate the magnitude of antiferromagnetic coupling the magnetic susceptibility data were fitted to the Bleaney Bowers equation $\chi_M T = 2Ng^2\beta^2/k[3 + \exp(-J/kT)]$ for two interacting copper(II) ions $(S = ½)$ with the Hamiltonian in the form $H = -JS_1S_2$. The magnetic data fitting with the above equation affords the parameters $J = -35.05$ cm^{-1} with $g = 2.10$.

Table 9
Electronic absorption data upon addition of CT-DNA to the complexes.

Complex	λ_{max} (nm)		Δλ	H (%)	K_b (M^{-1})
	Free	bound			
Complex **1**	366	351	15	−16.07	9.91×10^6
Complex **2**	332	330	02	08.21	9.25×10^6
Complex **3**	348	344	04	−09.64	8.68×10^6
Complex **4**	341	342	01	06.23	8.36×10^6
Complex **5**	368	361	07	11.23	2.24×10^5
Complex **6**	352	349	03	18.21	1.25×10^5
Complex **7**	346	344	02	−12.25	1.68×10^5
Complex **8**	341	342	01	16.36	1.15×10^5

The structural data for compound **6** indicate that the bridging oxygen atoms of phenolic moieties connected in an apical position to both the copper ions. As a consequence, there is no overlap with the magnetic orbitals of the metal centres and the exchange interaction through this bridging ligand is expected to be very weak.

3.4. Electrochemical studies

Redox behavior of the copper(II) complexes has been investigated by cyclic voltammetry using 0.1 M tetrabutylammonium-hexaflourophosphate (TBAHEP) as supporting electrolyte. The cyclic voltammetric profile of $[Cu(HAPPEN)(H_2O)_2]NO_3$ is given in Fig. 10. The electrochemical data of copper(II) complexes are presented in Table 7.

Repeated scans at various scan rates suggest that the presence of stable redox species in solution. $E_{1/2}$ values of **1–4** complexes observed at potential range of 0.122–0.397 V versus Ag/AgCl [58–60]. These values vary in the range of 0.322–0.397 V versus. Ag/AgCl for dinuclear complexes. It may be inferred that all the Cu (II) complexes undergo reduction to their respective Cu(I) complexes. The non-equivalent current in cathodic and anodic peaks (i_c/i_a = 1.192–1.801 for **1–4** and 0.326–0.812 for **5–8** at 100 mV s^{-1})

Table 7
Cyclic voltammetric data of complexes.

Complex	CV cathodic (E_{pc})	CV anodic (E_{pa})	ΔE_p	$E_{1/2}$	$-i_c/i_a$ (mV)	Log K_c[a] (V)	ΔG^o [b]
Complex **1**	0.268	0.526	258	0.397	1.268	0.130	747
Complex **2**	0.292	0.446	154	0.369	1.192	0.218	1251
Complex **3**	−0.104	0.446	550	0.171	1.658	0.061	350
Complex **4**	−0.020	0.265	285	0.122	1.801	0.117	672
Complex **5**	0.168	0.626	458	0.397	0.326	0.073	420
Complex **6**	0.146	0.582	436	0.364	0.452	0.077	442
Complex **7**	0.218	0.546	328	0.382	0.658	0.102	588
Complex **8**	0.107	0.537	285	0.322	0.812	0.117	676

[a] $\text{Log}\,K_c = 0.434\ ZF/RT\Delta E_p$.
[b] $\Delta G^o = -2.303\ RT \log K_c$.

Table 8
Details of electronic spectral titrations of DNA binding activity of complexes.

S. No.	Addition of DNA (μL)	Total volume of DNA (μL)	Total volume of solution (μL)	Conc. of complex (μM)	Conc. of DNA (μM)	r = [complex]/[DNA]
1	0	0	2000	20	0	
2	10	10	2010	19.9	3.0547	6.51
3	10	20	2020	19.801	6.0792	3.25
4	10	30	2030	19.704	9.0738	2.171
5	10	40	2040	19.607	12.0392	1.628
6	10	50	2050	19.512	14.9756	1.303
7	10	60	2060	19.417	17.8835	1.086
8	10	70	2070	19.323	20.7632	0.931
9	10	80	2080	19.231	23.6153	0.844
10	10	90	2090	19.138	26.4401	0.724

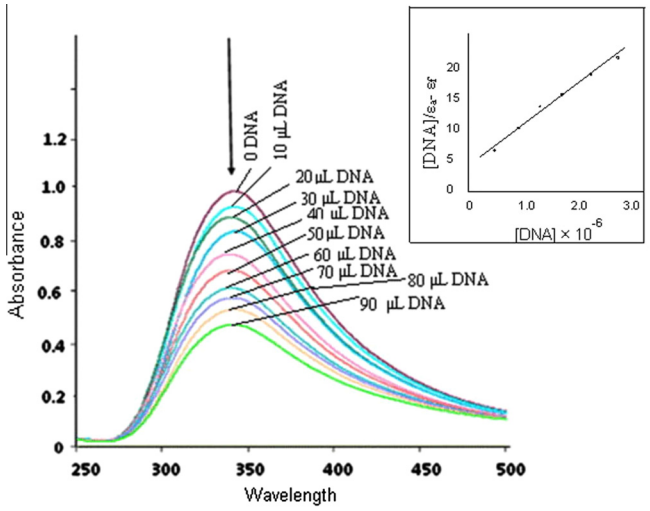

Fig. 11. Absorption spectra of complex **7** in the absence and in the presence of increasing concentration of CT-DNA; top most spectrum is recorded in the absence of DNA and below spectra on addition of 10 µl DNA each time; A plot of [DNA]/$(\varepsilon_a - \varepsilon_f)$ vs. [DNA] is shown in the inset.

indicate quasi-reversible behavior [61]. The difference ΔE_p in all the complexes exceeds the Nerstian requirement $59/n$ mV (n = number of electrons involved in oxidation reduction) which suggests quasi-reversible character associated with a considerable reorganization of the coordination sphere during electron transfer [62]. The complexes have large separation between anodic and cathodic peaks indicating quasi-reversible character. The $E_{1/2}$ values of copper complexes are inversely related to the size of the complex.

3.5. DNA binding studies

The interaction of metal complexes with calf-thymus DNA was monitored by UV–visible spectroscopy. The absorption spectra of complexes in aqueous solutions were compared in the absence and in the presence of CT-DNA. Absorption spectra were recorded in the range of 250–500 nm. The details of electronic spectral titrations of DNA binding activity of complexes are given in Table 8. Electronic absorption spectral data upon addition of CT-DNA and binding constants of these complexes are given in the Table 9. In the presence of increasing amounts of CT-DNA, the UV–Visible absorption spectra of mononuclear complexes **1**–**4** show bathochromic shift (λ_{max}: 1–15 nm). The spectra of all the complexes except complexes **1**, **3** and **7** showed an increase in absorbance (Hyperchromism). The three complexes showed a decrease in intensity exhibiting hypochromism. It is evident from the table, that all the complexes bind with DNA with high affinities and, the estimated binding constants are in the range 8–9 $\times 10^6$ M^{-1},-whereas the dinuclear complexes **5**–**8** show bathochromic shift (λ_{max}: 1–7 nm) and binding constants as in the range of 1.15–2.24 $\times 10^5$ M^{-1}. The change in absorbance values with increasing amounts of CT-DNA was used to evaluate the intrinsic binding constant K_b, for the complexes. Typical absorption spectra of $[Cu(HAPMEN)]_2(ClO_4)_2$ in presence and in absence of DNA are shown in Fig. 11. The binding constants (K_b) for DNA interaction of the complexes have been calculated by using the relation $[DNA]/(\varepsilon_a - \varepsilon_f) = [DNA]/(\varepsilon_b - \varepsilon_f) + 1/K_b(\varepsilon_b - \varepsilon_f)$ where [DNA] is the molar concentration of DNA, ε_a, ε_b and ε_f are apparent extinction coefficient ($A_{abs}/[M]$), the extinction coefficient for the complex in fully bound form and the extinction coefficient for free metal ion respectively.

Binding affinity of metal complexes decreases with increasing molecular weight; this may be due to the steric hindrance of bulky moieties present in the organic ligands. Also the binding constants of the dinuclear complexes are less than those of mononuclear copper(II) complexes. This may be due to the bulky nature of dinuclear complexes. Also the presence of good leaving groups (H_2O molecules) in mononuclear complexes causes the higher binding affinity towards DNA. Since the binding constants are high 10^5–10^6 M^{-1}), the complexes may be regarded as efficient intercalaters of DNA.

3.6. DNA cleavage activities

Nuclease activity of mono and dinuclear complexes derived from tridentate Schiff base ligands has been studied by agarose gel electrophoresis using pBR 322 plasmid DNA in Tris–HCl/NaCl (50 mM/5 mM) buffer (pH-7) in the presence and absence of H_2O_2 after 30 min incubation period at 37 °C. Concentration effect has been studied with the complex $[Cu(SAPEN)]_2(ClO_4)_2$ (complex **6**) from 100 to 250 µM. In presence of H_2O_2 all the super coiled DNA (form 1) is changed into nicked form (form II), which was further cleaved into linear form i.e., form III. From the experiments it is known that at higher concentrations, the complex exhibited significant DNA cleavage activity even in the absence of an oxidant, which may be due to catalytic hydrolysis [36]. Fig. 12 (a) and (b) show the cleavage activity of mononuclear copper(II) complexes. In presence of H_2O_2 the complexes cleave DNA more effectively (even lanes except lane 2), which may be due to the reaction of hy-

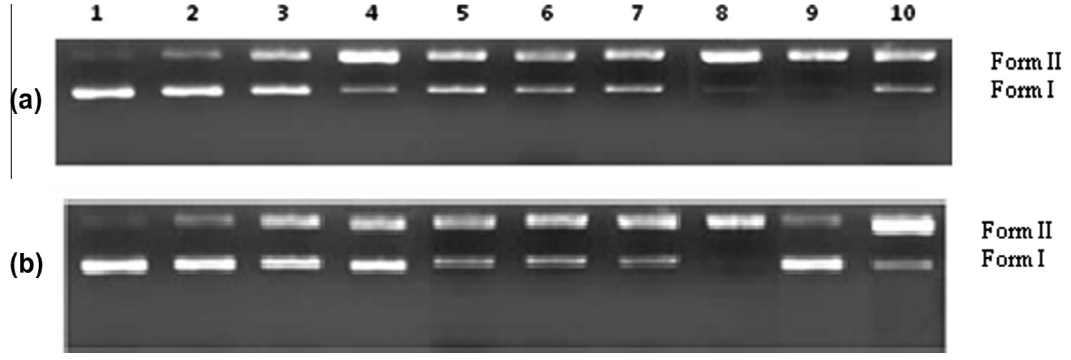

Fig. 12. Agarose gel (0.8%) showing results of electrophoresis of 1 µl of pBR 322 Plasmid DNA; 4 µl of Tris–HCl/NaCl (50 mM/5 mM) buffer (pH-7); 2 µl of complex in DMF(1×10^{-3} M); 11 µl of sterilized water; 2 µl of H_2O_2 (total volume 20 µl) were added, respectively, incubated at 37 °C (30 min); (a) *Mononuclear complexes: Lane 1*: DNA control; *Lane 2*: DNA control + H_2O_2; *Lane 3*: complex **1** + DNA; *Lane 4*: complex **1** + DNA + H_2O_2; *Lane 5*: complex **1** + DNA + EDTA; *Lane 6*: complex **1** + DNA + DTT; *Lane 7*: complex **3** + DNA; *Lane 8*: complex **3** + DNA + H_2O_2; *Lane 9*: complex **3** + DNA + EDTA; *Lane 10*: complex **3** + DNA + DTT; (b) *Lane 1*: DNA control; *Lane 2*: DNA control + H_2O_2; *Lane 3*: complex **2** + DNA; *Lane 4*: complex **2** + DNA + H_2O_2; *Lane 5*: complex **2** + DNA + EDTA; *Lane 6*: complex **2** + DNA + DTT; *Lane 7*: complex **4** + DNA; *Lane 8*: complex **4** + DNA + H_2O_2; *Lane 9*: complex **4** + DNA + EDTA; *Lane 10*: complex **4** + DNA + DTT;

droxyl radical with DNA. The percentage of the three forms of DNA is presented in Tables 10 and 11. From the data it is clear that percentage of cleavage activity of mononuclear copper complexes follows the order $[Cu(HAPMEN)(H_2O)_2]NO_3$ > $[Cu(HAPPEN)(H_2O)_2]NO_3$ > $[Cu(SAMEN)(H_2O)_2]NO_3$ > $[Cu(SAPEN)(H_2O)_2]NO_3$. Fig. 13(a) and (b) show the cleavage activity of dinuclear copper(II) complexes. These complexes also cleave DNA more effectively in presence of H_2O_2 the complexes cleave DNA more effectively. Quantification of the gel afforded data of three forms is presented in Tables 12 and 13. From the data it is clear that percentage of cleavage activity of dinuclear copper complexes follows the order $[Cu(HAPPEN)]_2(ClO_4)_2$ > $[Cu(HAPMEN)]_2(ClO_4)_2$ > $[Cu(SAPEN)]_2(ClO_4)_2$ > $[Cu(SAMEN)]_2(ClO_4)_2$. Further more it is clear that dinuclear complexes exhibit higher nuclease activity when compared with those of mononuclear complexes. Figs. 12 and 13 and Tables 10, 11 and 13 reveal that dinuclear complexes cleave DNA more effectively as the nicked form (form II) was further cleaved into linear form (form III).

Nuclease activity of complexes was also investigated in presence of chelating agent EDTA (1×10^{-6} M) and reducing agent DTT (1×10^{-6} M). In the absence of H_2O_2 the complexes cleaved supercoiled DNA (Form 1) into nicked DNA (Form II). From Figs. 12 and 13 it is evident that copper complexes cleave DNA more effectively in the presence of oxidant which may be due to hydroxyl radical (OH) reaction with DNA [63]. Chelating agent EDTA diminishes the nuclease activity of copper complexes, whereas in presence of reducing agent (DTT) the cleavage activity of copper complexes is enhanced. This may be due to formation of copper(I) complex by catalytic reduction. In presence of chelating agent EDTA the cleavage activity of the complexes was considerably reduced.

Table 10
Selected SC pBR322 DNA cleavage data of copper complexes in Fig. 11(a).

Lane No	Reaction condition	Percentage of		
		Form I	Form II	Form III
1	DNA	94.12	5.88	ND
2	DNA + H_2O_2 (10 μM)	91.33	8.67	ND
3	DNA + complex **1** (62.5 μM)	76.25	23.75	ND
4	DNA + complex **1** (62.5 μM) + DNA + H_2O_2 (10 μM)	22.92	75.65	1.43
5	DNA + complex 1 (62.5 μM) + EDTA (10 μM)	58.32	41.68	ND
6	DNA + complex **1** (62.5 μM) + DTT (10 μM)	51.44	49.56	ND
7	DNA + complex **3** (62.5 μM)	52.13	47.87	ND
8	DNA + complex **3** (62.5 μM) + H_2O_2 (10 μM)	21.79	76.22	1.99
9	DNA + complex **3** (62.5 μM) + EDTA(10 μM)	28.30	74.70	ND
10	DNA + complex **3** (62.5 μM) + DTT(10 μM)	37.26	62.74	ND

Table 11
Selected SC pBR322 DNA cleavage data of copper complexes in Fig. 11(b).

Lane No	Reaction condition	Percentage of		
		Form I	Form II	Form III
1	DNA	96.15	3.85	ND
2	DNA + H_2O_2 (10 μM)	91.64	8.36	ND
3	DNA + complex **2** (62.5 μM)	74.29	25.71	ND
4	DNA + complex **2** (62.5 μM) + DNA + H_2O_2 (10 μM)	48.14	51.90	ND
5	DNA + complex **2** (62.5 μM) + EDTA (10 μM)	52.63	47.36	ND
6	DNA + complex **2** (62.5 μM) + DTT (10 μM)	44.46	55.54	ND
7	DNA + complex **4** (62.5 μM)	50.92	49.07	ND
8	DNA + complex **4** (62.5 μM) + H_2O_2 (10 μM)	22.36	78.63	ND
9	DNA + complex **4** (62.5 μM) + EDTA (10 μM)	50.46	49.54	ND
10	DNA + complex **4** (62.5 μM) + DTT (10 μM)	29.43	70.56	ND

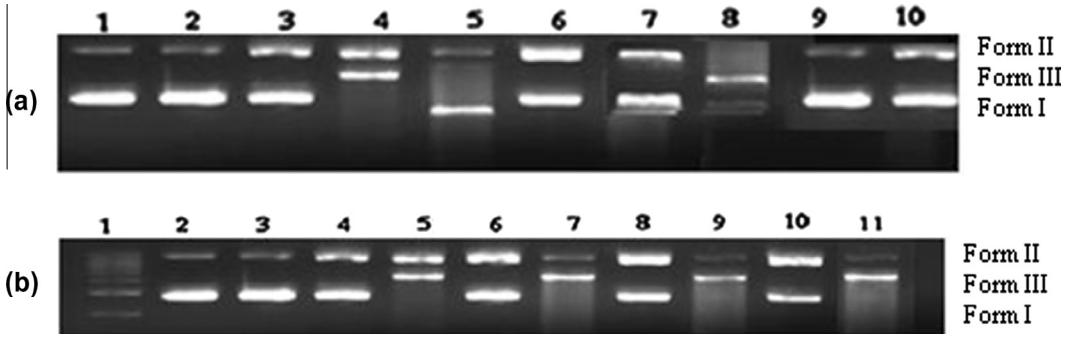

Fig. 13. Agarose gel (0.8%) showing results of electrophoresis of 1 μl of pBR 322 Plasmid DNA; 4 μl of Tris–HCl/NaCl (50 mM/5 mM) buffer (pH-7); 2 μl of complex in DMF(1×10^{-3} M); 11 μl of sterilized water; 2 μl of H_2O_2 (total volume 20 μl) were added, respectively, incubated at 37 °C (30 min); (a) *Dinuclear complexes: Lane 1*: DNA control; *Lane 2*: DNA control + H_2O_2; *Lane 3*: complex **5** + DNA; *Lane 4*: complex **5** + DNA + H_2O_2; *Lane 5*: complex **5** + DNA + EDTA; *Lane 6*: complex **5** + DNA + DTT; *Lane 7*: complex **7** + DNA; *Lane 8*: complex **7** + DNA + H_2O_2; *Lane 9*: complex **7** + DNA + EDTA; *Lane 10*: complex **7** + DNA + DTT; (b) *Lane 1*: DNA control; *Lane 2*: DNA control + H_2O_2; *Lane 3*: complex **6** + DNA; *Lane 4*: complex **6** + DNA + H_2O_2; *Lane 5*: complex **6** + DNA + EDTA; *Lane 6*: complex **6** + DNA + DTT; *Lane 7*: complex **7** + DNA; *Lane 8*: complex **7** + DNA + H_2O_2; *Lane 9*: complex 7 + DNA + EDTA; *Lane 10*: complex **7** + DNA + DTT;

Table 12
Selected SC pBR322 DNA cleavage data of copper complexes in Fig. 12(a).

Lane No	Reaction condition	Percentage of		
		Form I	Form II	Form III
1	DNA	96.32	3.68	ND
2	DNA + H_2O_2 (10 μM)	92.66	7.34	ND
3	DNA + complex **5** (62.5 μM)	53.82	46.18	ND
4	DNA + complex **5** (62.5 μM) + DNA + H_2O_2 (10 μM)	20.96	43.83	35.21
5	DNA + complex **5** (62.5 μM) + EDTA (10 μM)	63.33	36.68	ND
6	DNA + complex **5** (62.5 μM) + DTT (10 μM)	55.20	44.80	ND
7	DNA + complex **7** (62.5 μM)	50.48	49.52	ND
8	DNA + complex **7** (62.5 μM) + H_2O_2 (10 μM)	24.04	30.76	45.19
9	DNA + complex **7** (62.5 μM) + EDTA (10 μM)	80.77	19.23	ND
10	DNA + complex **7** (62.5 μM) + DTT (10 μM)	44.23	39.33	16.44

Table 13
Selected SC pBR322 DNA cleavage data of copper complexes in Fig. 12 (b).

Lane No	Reaction condition	Percentage of		
		Form I	Form II	Form III
2	DNA	97.33	2.67	ND
3	DNA + H_2O_2 (10 μM)	94.35	5.65	ND
4	DNA + complex **6** (62.5 μM)	64.92	35.08	ND
5	DNA + complex **6** (62.5 μM) + DNA + H_2O_2 (10 μM)	21.66	35.92	42.42
6	DNA + complex **6** (62.5 μM) + EDTA (10 μM)	49.47	50.53	ND
7	DNA + complex **6** (62.5 μM) + DTT (10 μM)	28.11	21.06	47.91
8	DNA + complex **8** (62.5 μM)	51.04	48.96	ND
9	DNA + complex **8** (62.5 μM) + H_2O_2 (10 μM)	23.70	20.00	56.30
10	DNA + complex **8** (62.5 μM) + EDTA (10 μM)	49.98	47.91	2.11
11	DNA + complex **8** (62.5 μM) + DTT (10 μM)	25.25	26.32	48.42

4. Conclusions

Water soluble mono and dinuclear copper(II) complexes of novel tridentate ligands have been synthesized and characterized. Physico-chemical and spectral studies reveal that mono nuclear complexes have square pyramidal structure, whereas the dinuclear complexes have square planar geometry. X-ray diffraction studies confirm the suggested structures. Mononuclear complexes show higher binding affinity towards CT-DNA when compared with dinuclear complexes possibly due to the presence of labile aqua ligands. In presence of H_2O_2 the complexes cleave DNA more effectively which may be due to the reaction of hydroxyl radical with DNA. All the complexes cleave DNA via oxidative path. Dinuclear complexes exhibit higher nuclease activity when compared with those of mononuclear complexes Nuclease activity is enhanced with higher nuclearity of the copper complexes. The highlights of the present investigations are: (i) The structures of the complexes are determined by single crystal X-ray diffraction studies, (ii) Both mono and dinuclear complexes are synthesized with given tridentate ligand. (iii) Solubility of present complexes is an attractive feature to develop chemotherapeutic drug. (iv) DNA binding and cleavage activities of the complexes are investigated. Mononuclear complexes bind DNA more strongly than corresponding dinuclear complexes possibly due to the labile aqua ligands indicating that the former complexes may bind DNA bases via substitution. Dinuclear complexes exhibit higher nuclease activity when compared with those of mononuclear complexes. The present observation is consistent with the idea that as nuclearity complex increases, DNA cleavage activity increases.

Acknowledgements

One of the authors (M. Pragathi) is thankful to UGC, SERO, Hyderabad for awarding teacher fellowship under Faculty Development Programme. The authors are thankful to DST, New Delhi (Sanction No. SR/S1/IC-37/2007) for financial support and to SAIF, IIT-Bombay for providing ESR spectral data. We are also thankful to SAIF, IIT-Madras for providing X-ray crystallographic data and VSM measurements. The authors also thank UGC and DST for providing equipment facility under SAP and FIST programs respectively.

Appendix A. Supplementary material

CCDC 892541 and 892618 contains the supplementary crystallographic data for **3** and **6**. These data can be obtained free of charge from The Cambridge Crystallographic Data Centre via www.ccdc.cam.ac.uk/data_request/cif. Supplementary data associated with this article can be found, in the online version, at http://dx.doi.org/10.1016/j.ica.2014.01.010.

References

[1] Y.B. Zeng, N. Yang, W.S. Liu, N. Tang, J. Inorg. Biochem. 97 (2003) 258.
[2] A.M. Pyle, T. Morii, J.K. Barton, J. Am. Chem. Soc. 112 (1990) 9432.
[3] J.K. Barton, J.M. Goldberg, C.V. Kumar, N.J. Turro, J. Am. Chem. Soc. 108 (1986) 2081.
[4] S. Mahadevan, M. Palaniandavar, Inorg. Chim. Acta 254 (1997) 291.
[5] S.J. Lippard, Acc. Chem. Res. 11 (1978) 211.
[6] S.M. Hech, Acc. Chem. Res. 19 (1986) 383.
[7] B. Lippert, Cisplatin: Chemistry and Biochemistry of a Leading Anticancer Drug, Wiley Interscience, 1999. p. 183.
[8] A.S. Abu-Surrah, M. Kettunen, Curr. Med. Chem. 13 (2006) 1337.
[9] C.S. Allardyce, P.J. Dyson, Platinum Met. Rev. 45 (2001) 62.
[10] I. Ott, R. Gust, Arch. Pharm. Chem. Life 340 (2007) 117.
[11] M.A. Jakupec, M. Galanski, V.B. Arion, C.G. Hartinger, B.K. Keppler, Dalton Trans. (2008) 183.
[12] P. Yang, M. Guo, Coord. Chem. Rev. 185 (1999) 189.
[13] S.K. Hadjikakou, N. Hadjiliadis, Coord. Chem. Rev. 253 (2009) 235.
[14] K. Strohfeldt, M. Tacke, Chem. Soc. Rev. 37 (2008) 1174.
[15] P.M. Abeysinghe, M.M. Harding, Dalton Trans. (2007) 3474.
[16] R. Gust, D. Posselt, K. Sommer, J. Med. Chem. 47 (2004) 5837.
[17] C.G. Hartinger, P.J. Dyson, Chem. Soc. Rev. 38 (2009) 391.
[18] M.B. Ferrari, F. Bisceglie, G.G. Favaa, G. Pelosia, P. Tarasconi, R. Albertini, S. Pinelli, J. Inorg. Biochem. 89 (2002) 36.

[19] M.B. Ferrari, F. Bisceglie, G. Pelosi, P. Tarasconia, R. Albertini, A. Bonati, P. Lunghi, S. Pinelli, J. Inorg. Biochem. 83 (2001) 169.
[20] M.R. Arguelles, M.B. Ferrari, F. Biscegli, C. Pelizzi, G. Pelosi, S. Pinelli, M. Sassi, J. Inorg. Biochem. 98 (2004) 313.
[21] M.B. Ferraria, F. Bisceglie, A. Buschini, S. Franzoni, G. Pelosi, S. Pinelli, P. Tarasconi, M. Tavone, J. Inorg. Biochem. 104 (2010) 199.
[22] E. Bouwman, W.L. Driessen, J. Reedijk, Coord. Chem. Rev. 104 (1990) 143.
[23] K.D. Karlin, Z. Tyeklár, Adv. Inorg. Biochem. 9 (1994) 123.
[24] N. Kitajima, Y. Moro-oka, Chem. Rev. 94 (1994) 737.
[25] E.I. Solomon, U.M. Sundaram, T.E. Machonkin, Chem. Rev. 96 (1996) 2563.
[26] W.B. Tolman, Acc. Chem. Res. 30 (1997) 227.
[27] G.Y.S.K. Swamy, K. Ravikumar, K. Chandramohan, N.V. Lakshmi, Cryst. Res. Technol. 36 (2001) 1273.
[28] J.-P. Costes, F. Dahan, M.B.F. Fernandez, M.F.I. Garcia, A.M.G. Deibe, J. Sanmarth, Inorg. Chim. Acta 274 (1998) 73.
[29] J.P. Costes, J.F. Serra, F. Dahan, J.P. Laurent, Inorg. Chem. 25 (1986) 2790.
[30] J.P. Costes, F. Dahan, J.P. Laurent, Inorg. Chem. 25 (1986) 413.
[31] A. Erxleben, Inorg. Chem. 40 (2001) 208.
[32] P. Haribabu, Ph.D., thesis, Sri Krishnadevaraya University, Anantapur, Andhra Pradesh, 2011.
[33] K. Hussain Reddy, P. Sambasiva Reddy, P. Ravindra Babu, J. Inorg. Biochem. 21 (1999) 169.
[34] M. Surendra Babu, K. Hussain Reddy, P.G. Krishna, Polyhedron 26 (2007) 572.
[35] P. Murali Krishna, K. Hussain Reddy, Inorg. Chim. Acta 362 (2009) 4185.
[36] P. Murali Krishna, K. Hussain Reddy, J.P. Panday, D. Dayananda, Transition Met. Chem. 33 (2008) 661.
[37] P. Haribabu, Y. Patil, K. Hussain Reddy, M. Nethaji, Inorg. Chim. Acta 392 (2012) 478.
[38] Siemens, SMART and SAINT, Area Detector Control and Integration Software, Siemens Analytical X-ray Instruments Inc., Madison, Wisconsin, USA, 1996.
[39] G.M. Sheldrick, Acta Crystallogr., Sect. A 46 (1990) 467.
[40] G.M. Sheldrick, SHELXS-97 Program for the Solution of Crystal Structures, University of Gottingen, Germany, 1997.
[41] K. Brandenburg, H. Putz, DIAMOND version 3.0 Crystal Impact, GbR, Postfach 1251, D-53002 Bonn, Germany, 2004.
[42] W.J. Geary, Coord. Chem. Rev. 7 (1971) 81.
[43] B.J. Hathaway, in: G. Wilkinson, R.D. Gillard, J.A. Mecleverty (Eds.), Comprehensive Coordination Chemistry, vol. 5, Pergfamon, Oxford, 1987, p. 583.
[44] A.K. Patra, M. Ray, R. Mukharjee, J. Chem. Soc., Dalton Trans. 15 (1999) 2461.
[45] R.N. Patel, N. Singh, D.K. Patel, V.L.N. Gundla, Indian J. Chem. 46A (2007) 422.
[46] B. Keshavan, P.G. Chandrashekara, N.M. Made, J. Mol. Struct. 553 (2000) 193.
[47] B. Sarkar, M.S. Ray, M.G.B. Drew, A. Figuerola, C. Diaz, A. Ghosh, Polyhedron 25 (2006) 3084.
[48] B. Sarkar, M.S. Ray, Y.-Z. Li, Y. Song, A. Figuerola, E. Ruiz, J. Cirera, J. Cano, A. Ghosh, Chem. Eur. J. 13 (2007) 9297.
[49] B.J. Hathaway, D.E. Billing, Coord. Chem. Rev. 5 (1961) 143.
[50] S. Tyagi, B.J. Hathaway, J. Chem. Soc., Dalton Trans. 10 (1981) 2029.
[51] E. Vinuelas-Zahinos, M.A. Maldonado-Rogado, F. Luna-Giles, F.J. Barros-Garcia, Polyhedron 27 (2008) 879–886.
[52] V. Sagakuchi, A.W. Addison, J. Chem. Soc., Dalton Trans. 4 (1979) 600.
[53] D. Kivelson, R. Neiman, J. Chem. Phys. 35 (1961) 149.
[54] P.A.N. Reddy, M. Nethaji, A.R. Chakravarthy, Eur. J. Inorg. Chem. 12 (2003) 2318.
[55] V. Philip, V. Suni, M.R.P. Kurup, M. Nethaji, Polyhedron 24 (2005) 1133.
[56] P. Talukder, S. Sen, S. Mitra, L. Dahlenberg, C. Desplanches, J.-P. Sutter, Eur. J. Inorg. Chem. 2 (2006) 329.
[57] C. Biswas, M.G.B. Grew, S. Asthana, C. Desplanches, A. Ghosh, J. Mol. Struct. 965 (2010) 39.
[58] X.H. Bu, Z.H. Zhang, X. Cao, S. Ma, Y. Tichen, Polyhedron 16 (1997) 3525.
[59] S. Dhar, D. Senapathi, P.K. Das, P. Chattopadyay, M. Nethaji, A.R. Chakravarthy, J. Am. Chem. Soc. 125 (2003) 12218.
[60] S. Djebbar-Sid, O. Benali-Baitich, J.P. Deloume, Polyhedron 16 (1997) 2175.
[61] A.A. Khumhar, S.B. Rendye, D.X. West, A.E. Libert, Transition Met. Chem. 16 (1991) 276.
[62] S. Usha, M. Palaniandavar, J. Chem. Soc., Dalton Trans. 15 (1994) 2277.
[63] A. Hangan, A. Bodiki, L. Oprean, G. Alzuet, M.L. Gpnzalez, J. Borras, Polyhedron 29 (2010) 1305.